Spin Noise Spectroscopy of a Single Spin Using Single Detected Photons

M. Gundín,[1,†] P. Hilaire,[1,†] C. Millet,[1,†] E. Mehdi,[1,2] C. Antón,[1,3] A. Harouri,[1] A. Lemaître,[1] I. Sagnes,[1] N. Somaschi,[4] O. Krebs,[1] P. Senellart,[1] and L. Lanco[1,2,5,*]

[1]*Université Paris-Saclay, CNRS, Centre de Nanosciences et de Nanotechnologies, 91120 Palaiseau, France*
[2]*Université Paris Cité, Centre de Nanosciences et de Nanotechnologies, 91120 Palaiseau, France*
[3]*Departamento de Física de Materiales, Instituto Nicolás Cabrera, Instituto de Física de la Materia Condensada, Universidad Autónoma de Madrid, 28049 Madrid, Spain*
[4]*Quandela, 7 rue Leonard de Vinci, 91300 Massy, France*
[5]*Institut Universitaire de France (IUF), 75005 Paris, France*

(Received 3 April 2024; accepted 15 November 2024; published 24 January 2025)

Spin noise spectroscopy has become a widespread technique to extract information on spin dynamics in atomic and solid-state systems, in a potentially nonperturbative way. Here we experimentally demonstrate a new approach in spin noise spectroscopy, based on the detection of single photons. Because of the large spin-dependent polarization rotations provided by a deterministically coupled quantum dot-micropillar device, giant spin noise signals induced by a single-hole spin are extracted in the form of photon-photon cross-correlations. Ultimately, such a technique can be extended to an ultrafast regime probing mechanisms down to few tens of picoseconds.

DOI: 10.1103/PhysRevLett.134.036902

Quantum systems are inherently subject to noise arising from their coupling to an environment, which represents a challenge for quantum technologies [1–3]. Spin noise spectroscopy (SNS) [4] has emerged in this context as a powerful tool to probe the dynamics of atomic [5] and solid-state [6] spins. Standard optical SNS typically involves measuring polarimetric signals, such as Faraday-Kerr polarization rotations or circular dichroism, which are proportional to the internal magnetization [7]. Measuring the noise power spectrum of such signals allows retrieving the information on their temporal correlations, and thus, on the temporal correlations of the system's magnetization, governed by the internal spin dynamics [8]. A strong advantage of such a method is that it can potentially be nonperturbative, probing internal fluctuations within a system kept at thermal equilibrium [7].

Important advances were obtained in the last decade, including high-frequency SNS using pulsed lasers [9,10], heterodyne SNS detection [11–13], two-color SNS [14], access to temporal correlation functions beyond second-order [15], and beyond thermal equilibrium [16–19]. Yet, the low polarimetric signals imprinted by single spins [20] have limited most SNS experiments to spin ensembles, contrary to perturbative techniques typically used to study single-spin relaxation [21,22] and decoherence [23,24]. A promising route to implement SNS with single spins relies on the enhancement of polarimetric signals [25–27].

Yet, only a few pioneering experiments of single-spin SNS could be reported, using planar microcavities [28–30]. Thus far, no experiments have been reported to enhance SNS in 3D-confining microcavities.

In this Letter, we report on a novel approach, measuring the spin noise (SN) signal induced by a single spin through the detection of single photons. Our technique takes advantage of the large polarization rotations induced by a charged quantum dot (QD) in a pillar microcavity [31–33]. We implement photon-photon cross-correlations, measured along optimized polarization bases, to demonstrate giant SN signals induced by a single hole spin. The experimental data are all reproduced by a complete numerical description of the system, taking into account the hyperfine interaction between the electron-in-trion and the surrounding nuclei, resulting in nontrivial spin dynamics [21,22]. The time-dependence of the cross-correlations provides direct access to the spin dynamics, i.e., the spin noise, circumventing the need to measure power spectra [28–30]. Additionally, the absolute amplitude of the measured correlators informs us on the environmental noise sources broadening the optical transitions [34], and on the measurement back-action induced on the system by the detection of a single photon. Ultimately, this approach paves the way towards single-spin SNS experiments above 10 GHz, limited only by the temporal jitter of single-photon detection.

The experiments we report are performed with the sample structure of Ref. [35], which allows optically injecting a single hole in an annealed InAs/GaAs QD [36] (see also Supplemental Material [37]). The spin dynamics

*Contact author: loic.lanco@u-paris.fr
†These authors contributed equally to this work.

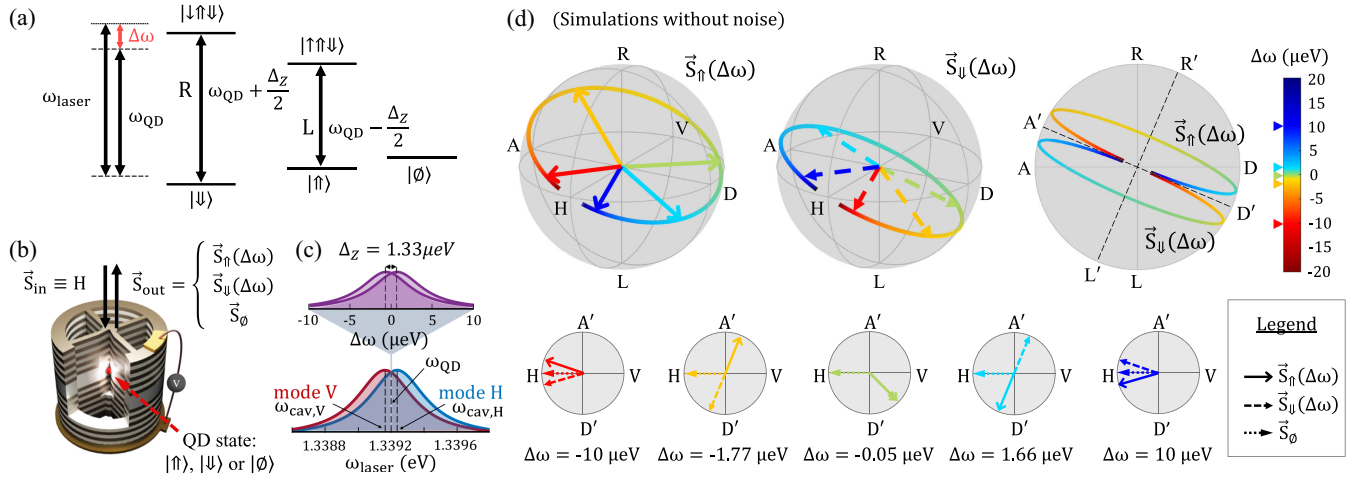

FIG. 1. (a) Energy level scheme of a positively charged quantum dot under a longitudinal magnetic field, inducing a Zeeman splitting Δ_Z. (b) The polarization $\vec{S}_{\text{out}}$ reflected by the micropillar depends on the QD state and on the QD-laser detuning $\Delta\omega$. (c) Frequency configuration of the QD transitions (top) compared with the cavity modes (bottom). (d) Numerical simulations, in the absence of noise, of the output polarization $\vec{S}_{\Uparrow}$ (upper left panel) and $\vec{S}_{\Downarrow}$ (upper middle panel), as a function of $\Delta\omega$. In the upper right panel, $\vec{S}_{\Uparrow}$ and $\vec{S}_{\Downarrow}$ are shown together, projected in a plane perpendicular to HV, highlighting symmetry axes A'D' and R'L' rotated with respect to AD and RL. The lower panels show the Stokes vectors $\vec{S}_{\Uparrow}$, $\vec{S}_{\Downarrow}$, and $\vec{S}_{\varnothing}$ for the same selected detunings, projected in the HV-A'D' plane.

and optical properties of this device are captured by the 5-level system in Fig. 1(a). The charged QD ground states (hole spin $|\Uparrow\rangle$ or $|\Downarrow\rangle$) are connected to the excited trion states, respectively $|\uparrow\Uparrow\Downarrow\rangle$ or $|\downarrow\Uparrow\Downarrow\rangle$, by circularly L or R polarized transitions [47]. As in previous works on single-spin SNS [28–30], a longitudinal magnetic field of 30 mT is applied to partially shield the spin from nuclear spin fluctuations. The degeneracy of the QD transition at $\omega_{\text{QD}} = 1.3392$ eV ($\hbar = 1$ units throughout the text) is lifted with a Zeeman splitting $\Delta_Z = 1.33$ μeV. A fifth empty state $|\varnothing\rangle$ represents the uncharged quantum dot. Both $|\Uparrow\rangle - |\uparrow\Uparrow\Downarrow\rangle$ and $|\Downarrow\rangle - |\downarrow\Uparrow\Downarrow\rangle$ transitions are excited by the same continuous-wave laser with energy ω_{laser}, detuned by $\Delta\omega = \omega_{\text{laser}} - \omega_{\text{QD}}$.

The micropillar cavity sketched in Fig. 1(b) has two modes M = H, V, corresponding to orthogonal linear polarizations defined as horizontal and vertical. The incoming polarization is described in the Poincaré sphere by the input Stokes vector $\vec{S}_{\text{in}}$, and we, respectively, denote $\vec{S}_{\Uparrow}$, $\vec{S}_{\Downarrow}$, and $\vec{S}_{\varnothing}$ the output Stokes vectors obtained conditionally to the system states $|\Uparrow\rangle$, $|\Downarrow\rangle$ and $|\varnothing\rangle$ [Fig. 1(b)]. We choose $\vec{S}_{\text{in}}$ along the cavity eigenaxis H, ensuring that $\vec{S}_{\varnothing} = \vec{S}_{\text{in}}$: the reflected polarization remains unrotated in absence of interaction with the QD. The cavity is birefringent, with mode energies $\omega_{\text{cav,H}}$ and $\omega_{\text{cav,V}}$ separated 74 ± 5 μeV, compared to the mode linewidths $\kappa_{\text{H}} = 420 \pm 20$ and $\kappa_{\text{V}} = 430 \pm 20$ μeV. The QD, slightly red-detuned 1.6 μeV from the central energy $(\omega_{\text{cav,H}} + \omega_{\text{cav,V}})/2$, is coupled efficiently to both modes [Fig. 1(c)]. These parameters, along with the cavity output coupling efficiency $\eta_{\text{top}} = 0.89 \pm 0.05$ for both modes, are extracted from separate polarization-resolved experiments performed when the system is in state $|\varnothing\rangle$ [37,48].

In the absence of noise induced on the optical transitions, and in the low-power limit, $\vec{S}_{\Uparrow}$ and $\vec{S}_{\Downarrow}$ are pure states that can be analytically derived [33,37]. They depend on the detunings between the laser, QD, and cavity energies; on the parameters κ_{H}, κ_{V}, and η_{top}; on the QD-mode coupling g (governing Purcell-enhanced emission in the cavity mode); and on the rate of spontaneous emission in other modes, γ_{sp}. Figure 1(d) displays the predicted vectors ($\vec{S}_{\Uparrow}$: upper left panel, $\vec{S}_{\Downarrow}$: upper central panel) in the absence of noise, for various detunings $\Delta\omega$ (see color scale and selection of detunings). These vectors are computed using previously mentioned parameter values, together with $g = 17.5 \pm 0.5$ and $\gamma_{\text{sp}} = 0.9 \pm 0.2$ μeV, these estimations being discussed later on.

As the excitation laser approaches resonance, $\vec{S}_{\Uparrow}$ and $\vec{S}_{\Downarrow}$ experience giant rotations around the sphere, governed by the interference between the coherent QD resonance fluorescence and the laser light directly reflected by the empty cavity [37]. The trajectories of the Stokes vectors $\vec{S}_{\Uparrow}(\Delta\omega)$ and $\vec{S}_{\Downarrow}(\Delta\omega)$, when $\Delta\omega$ is continuously varied, show a symmetric behavior highlighted in the upper right panel of Fig. 1(d). In this panel, the possible values of $\vec{S}_{\Uparrow}(\Delta\omega)$ and $\vec{S}_{\Downarrow}(\Delta\omega)$ are projected in the RL-AD plane (A/D: antidiagonal or diagonal polarization). It is convenient, however, to work with the symmetry axes R′L′ and A′D′, rotated 23° with respect to RL and AD, due to cavity birefringence [37]. In the bottom panel of Fig. 1(d), the

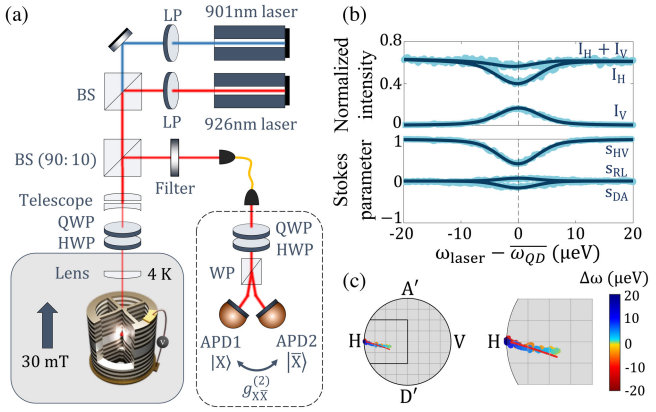

FIG. 2. (a) Experimental setup [linear polarizer (LP); nonpolarizing beam splitter (BS); quarter/half waveplate (QWP/HWP); Wollaston prism (WP); avalanche photodiodes (APD). (b) (Top) Normalized reflected intensities I_{H}, I_{V}, and $I_{\mathrm{H}}+I_{\mathrm{V}}$ as a function of the detuning between ω_{laser} and the average QD energy $\overline{\omega_{\mathrm{QD}}}$. (Bottom) Stokes parameters s_{HV}, s_{DA}, and s_{RL} of the reflected polarization state. (c) (Left) Reflected averaged polarization, projected on the HV-D′A′ plane. (Right) Zoom on the region of interest.

Stokes vectors $\vec{S}_{\Uparrow}$, $\vec{S}_{\Downarrow}$, and $\vec{S}_{\varnothing}$ are displayed as projections in the HV-A′D′ plane, for selected detunings (see legend). Close to resonance, the Stokes vectors can be drastically modified by a few μeV variation of $\Delta\omega$. For individual values of $\Delta\omega$, an asymmetry is observed between the orientations of $\vec{S}_{\Uparrow}$ and $\vec{S}_{\Downarrow}$ with respect to the HV axis, due to the Zeeman splitting.

We now turn to the optical setup in Fig. 2(a). A cw laser, tunable around 926 nm, is injected into the pillar microcavity with incoming powers between 4 and 64 pW, to probe the optical transitions in the linear, low-power regime [49]. A telescope, and a cold lens inside the cryostat ($T=4$ K), allow producing a laser spot size of 2 μm on the pillar surface, for an optimal injection in the cavity [48]. A set of quarter and half waveplates align the incoming polarization with the cavity eigenaxis. The reflected light is sent, via a R90-T10 nonpolarizing beam splitter and a single-mode fiber for spatial filtering, to a polarization analyzer. The latter, composed of a quarter-waveplate, a half-waveplate, and a Wollaston prism, allows separating any polarization X from its opposite $\bar{\mathrm{X}}$, directing them to two single-photon avalanche diodes. This setup is used both for reconstructing the output polarization [50] and measuring photon-photon cross-correlations. Undesired polarization rotations induced by the setup are compensated by slightly adjusting all waveplates. In addition to the tunable laser, a second-color CW laser at 901 nm, linearly polarized and with 4 μW power, is used to optically inject a hole spin in the quantum dot. It allows selectively exciting the neutral exciton transition, through a quasiresonance [35,37]. Whenever the QD is uncharged, this laser is used to populate the exciton state until a photoexcited electron escapes the QD, leaving a hole to populate the dot for typically 100 μs [35,37]. This laser is spectrally filtered out. Background counts, coming from dark counts and residual emission induced by the 901 nm laser, are subtracted from all our intensity and cross-correlation measurements [37].

In Fig. 2(b), we display the measured output intensities along H and V polarizations, normalized by the incoming intensity, as a function of $\omega_{\mathrm{laser}}-\overline{\omega_{\mathrm{QD}}}$, with $\overline{\omega_{\mathrm{QD}}}$ the average QD energy taking into account the inhomogeneous broadening of the optical transitions [34,37]. The peak signal in the intensity I_{V} corresponds to cross-polarized QD resonance fluorescence; the dip in I_{H} results from destructive interference between the directly reflected laser and the copolarized resonance fluorescence. Spectral wandering, i.e. slow fluctuations of the QD energy, broadens the emission line with a standard deviation $\sigma_{\mathrm{SW}}=2.6\pm0.5$ μeV (deduced from fits discussed later on) around the average energy $\overline{\omega_{\mathrm{QD}}}$.

Complete tomography of the output state is shown in the bottom panel of Fig. 2(b). The Stokes parameter s_{HV} is defined as $s_{\mathrm{HV}}=[(I_{\mathrm{H}}-I_{\mathrm{V}})/(I_{\mathrm{H}}+I_{\mathrm{V}})]$, with analogous definitions for s_{DA} and s_{RL}. In Fig. 2(c) we display the Stokes vector in the HV-D'A' plane, as a function of $\omega_{\mathrm{laser}}-\overline{\omega_{\mathrm{QD}}}$ [37]. The depolarization at QD-laser resonance comes from two effects. First, the lack of spin initialization, and the limited charge occupation probability of $75\%\pm5\%$ (studied separately, using cross-correlation measurements in the HV basis [35,37]), lead to a polarization state averaging contributions from $\vec{S}_{\Uparrow}$, $\vec{S}_{\Downarrow}$, and $\vec{S}_{\varnothing}$ [33]. Moreover, the value of σ_{SW} is large enough to induce an additional averaging over fluctuating vectors $\vec{S}_{\Uparrow}$ and $\vec{S}_{\Downarrow}$.

Intensity measurements provide information on the system's steady state, yet convey little information on the spin dynamics. In the following, we fix ω_{laser} and analyze the polarization fluctuations by measuring the cross-correlation function in basis $\mathrm{X}\bar{\mathrm{X}}$:

$$g^{(2)}_{\mathrm{X}\bar{\mathrm{X}}}(\tau)=\frac{P(\bar{\mathrm{X}},\tau|\mathrm{X},0)}{P(\bar{\mathrm{X}})}, \tag{1}$$

with $P(\bar{\mathrm{X}},\tau|\mathrm{X},0)$ the conditional probability to detect a photon in $\bar{\mathrm{X}}$ at time τ, knowing that a previous photon was detected in X at time 0, and $P(\bar{\mathrm{X}})$ the detection probability in $\bar{\mathrm{X}}$. Generalizing from Ref. [51], we use this function to define the (basis-dependant) correlator $C_{\mathrm{X}}(\tau)=1-g^{(2)}_{\mathrm{X}\bar{\mathrm{X}}}(\tau)$.

To interpret such quantities, let us consider an ideal case where $|\varnothing\rangle$ is not populated, where $\vec{S}_{\Uparrow}$ and $\vec{S}_{\Downarrow}$ correspond to opposite states in the Poincaré sphere, the measured states $\mathrm{X}/\bar{\mathrm{X}}$, respectively, pointing towards $\vec{S}_{\Uparrow}/\vec{S}_{\Downarrow}$. In such ideal case, an X-polarized detection indicates that the spin is $|\Uparrow\rangle$

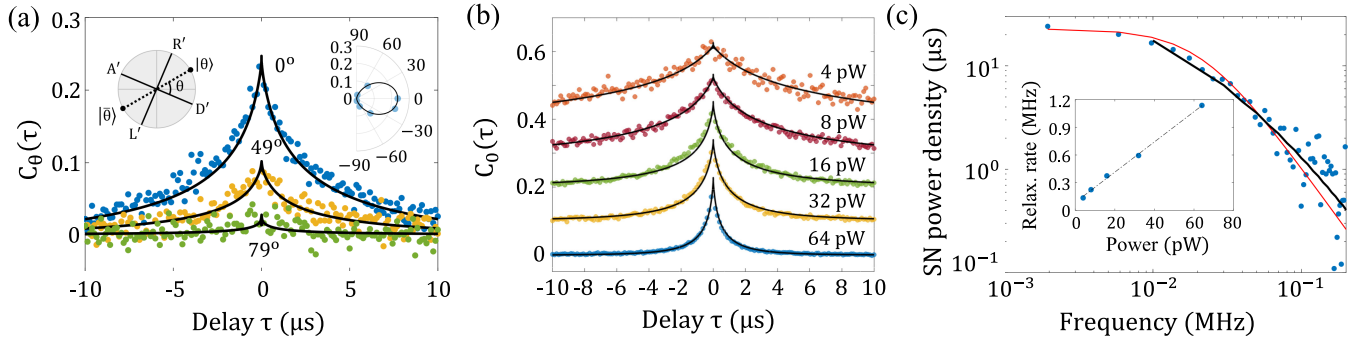

FIG. 3. (a) Correlator $C_\theta(\tau)$ measured in basis $\theta\bar{\theta}$ for various angles (see left inset): $\theta = 0°$ (blue dots), $\theta = 49°$ (yellow dots) and $\theta = 79°$ (green dots). Right inset: maximum signal $C_\theta(0)$ measured (blue dots) as a function of θ. (b) Correlator $C_0(\tau)$, for a fixed angle $\theta = 0°$, and for different laser powers. Each curve is vertically displaced by 0.1 for easier visualization. (c) SN spectrum, obtained through the FFT of the correlator $C_0(\tau)$, measured at 4 pW (blue dots: experimental data, red solid line: single Lorentzian fit of the SN spectrum). Inset: Effective spin relaxation rate increasing linearly with the excitation power. In all panels, solid black lines correspond to fits obtained with a single numerical model reproducing all experiments.

after detection (perfect measurement). Subsequent reflected photons will then be in the same polarization $\vec{S}_{\Uparrow}$, implying that no photon can be detected in $\bar{\mathrm{X}}$, hence $g^{(2)}_{\mathrm{X}\bar{\mathrm{X}}}(\tau) = 0$ and $C_{\mathrm{X}}(\tau) = 1$. Spin relaxation then leads to the correlator decaying towards $C_{\mathrm{X}}(\tau) = 0$. In such ideal case, $C_{\mathrm{X}}(\tau)$ matches the quantity of interest in SNS, i.e., the spin correlation function $\langle \hat{S}_z(\tau)\hat{S}_z(0)\rangle$ (with $\hat{S}_z$ the spin projection in the light beam direction [8]). Indeed $\langle \hat{S}_z(\tau)\hat{S}_z(0)\rangle$ also decays from $\langle \hat{S}_z^2\rangle = 1$ to $\langle \hat{S}_z\rangle\langle \hat{S}_z\rangle = 0$, with a dynamics governed by spin relaxation.

In practice, spectral wandering induces variations of $\Delta\omega$, even though ω_{laser} is fixed, so that $\vec{S}_{\Uparrow}$ and $\vec{S}_{\Downarrow}$ strongly fluctuate (see Fig. 1). Still, for some orientations of $\vec{S}_{\Uparrow}$ and $\vec{S}_{\Downarrow}$, and a properly chosen basis $\mathrm{X}\bar{\mathrm{X}}$, an X-polarized detection event may create a significant imbalance between the conditional probabilities for states $|\Uparrow\rangle$ and $|\Downarrow\rangle$. This, in turn, decreases the probability for subsequent photons to be measured in $\bar{\mathrm{X}}$, leading to intermediate cross-correlations at short delays $[0 < g^{(2)}_{\mathrm{X}\bar{\mathrm{X}}}(0) < 1]$, and thus, lower-than-unity values of $C_{\mathrm{X}}(0)$.

In Fig. 3(a), the measured correlator $C_\theta(\tau) = 1 - g^{(2)}_{\theta\bar{\theta}}(\tau)$ is plotted for $\omega_{\mathrm{laser}} = \overline{\omega_{\mathrm{QD}}}$, for different bases $\theta\bar{\theta}$ (theoretical fits are discussed later on). These bases, chosen in the D'A'-R'L' plane previously defined, are uniquely determined by the angle θ, measured with respect to the D'A' axis [left inset of Fig. 3(a)]. This choice ensures that both $|\theta\rangle$ and $|\bar{\theta}\rangle$ are perpendicular, in the Poincaré sphere, to $\vec{S}_{\varnothing} = |H\rangle$. As such, a detection event in polarization $|\theta\rangle$ does not modify the conditional probability to be in the state $|\varnothing\rangle$, and only modifies the imbalance between occupation probabilities for states $|\Uparrow\rangle$ and $|\Downarrow\rangle$. In such a case the relaxation dynamics of the correlator $C_\theta(\tau)$ is only governed by spin relaxation, as desired, and is kept insensitive to the charge dynamics [37]. The strength of this spin noise signal is described by the short-delay correlation value $C_\theta(0)$, reaching up to $C_0(0) = 0.25$ at $\theta = 0$. This value represents a giant SN signal, yet lower than the ideal maximum $C_0(0) = 1$. The angular dependence of $C_\theta(0)$ is displayed in the right inset of Fig. 3(a). Notably, $C_\theta(0)$ strongly decreases when θ approaches $\pi/2$. This highlights the importance of measuring along D'A' ($\theta = 0$), which allows best discriminating between $\vec{S}_{\Uparrow}$ and $\vec{S}_{\Downarrow}$ [see Fig. 1(d)], thus creating maximal imbalance between the conditional occupation probabilities for $|\Uparrow\rangle$ and $|\Downarrow\rangle$. Conversely, measuring along R'L' $[\theta = \pi/2]$ implies that $|\theta\rangle$ and $|\bar{\theta}\rangle$ are approximately perpendicular to $\vec{S}_{\Uparrow}$ and $\vec{S}_{\Downarrow}$ in the Poincaré sphere, which translates into a negligible imbalance of the conditional spin populations after detection.

After photon detection, the system's conditional density matrix evolves back to the steady state, yielding a progressive decay of $C_\theta(\tau)$. Figure 3(b) displays the correlator measured in the optimal D'A' basis, $C_0(\tau)$, for different incoming powers P_{in}, showing that the spin relaxation becomes faster at higher powers. This is typical in a positively charged quantum dot, where the hole spin lifetime is orders of magnitude larger than the electron-in-trion spin relaxation time [28,29]: spin-flip events occur predominantly between the two trion states, with a rate increasing with the trion occupation probability.

Before discussing the fits in Figs. 3(a) and 3(b), we display in Fig. 3(c) the Fourier transform of the correlator $C_0(\tau)$, equivalent to a spin noise spectrum [51], for $P_{\mathrm{in}} = 4$ pW. As a first approximation, the spectrum is tentatively fitted by a single Lorentzian (red solid line), following Ref. [28]. An effective, monoexponential spin relaxation rate is deduced from the Lorentzian full width at half maximum (FWHM), as $\Gamma^{(\mathrm{eff})} = \pi \times \mathrm{FWHM}$. This effective rate increases linearly with P_{in} (inset) and, thus, with the trion occupation probability. This confirms that

direct hole spin flips between $|\Uparrow\rangle$ and $|\Downarrow\rangle$ play a negligible role in the effective relaxation, which is dominated by the electron-in-trion, i.e., spin flips between $|\uparrow\Uparrow\Downarrow\rangle$ and $|\downarrow\Uparrow\Downarrow\rangle$. Extrapolating this linear fit to the low power limit, an intrinsic hole spin relaxation rate of 80 ± 30 kHz can be estimated, compared to several kHz measured in Ref. [28], also with a 31 mT longitudinal magnetic field yet with a nonannealed QD.

We now turn to our complete fits, performed with a numerical model solving the system's master equation, and reproducing all experiments with a single set of parameters [37]. This model allows computing the system's steady state density matrix (governing all fits in Fig. 2), as well as the conditional density matrix after photon detection, and its subsequent relaxation (governing all fits in Fig. 3) [37]. Instead of relying on the empiric description with a Lorentzian fit, our model explicitly takes into account the hyperfine interaction induced by nuclear spins, in the form of a frozen, randomly oriented Overhauser field [47], to which the electron-in-trion coherently couples (coupling strength $\gamma_e = 0.5 \pm 0.1$ μeV) [37]. In such a model, the electron spin precesses around an effective axis given by the sum of the Overhauser field and the longitudinal applied field. This leads, when averaging over all orientations of the Overhauser field, to a non-mono-exponential dynamics [52]. Following Refs. [53–55], we also introduce an additional isotropic electron spin relaxation time $\tau_e = 70 \pm 10$ ns to take into account a slower, monoexponential spin relaxation process which is not described by the purely frozen Overhauser field model [37]. In lack of significant experimental signatures, we did not include in this model the hole spin hyperfine interaction, nor any additional hole spin relaxation [37].

This global, fully numerical model, is found to reproduce all correlators in Figs. 3(a) and 3(b), and the SN spectra of Fig. 3(c) (black solid line), more realistically than empiric individual fits. In particular, the non-mono-exponential dynamics is apparent at short delays and, correspondingly, the high-frequency slope of the SN spectrum does not match the expected slope for a Lorentzian behavior. Interestingly, this numerical model also allows predicting absolute amplitudes for the correlators and SN spectra. The fit of these amplitudes, together with the fits of all Stokes and reflectivity measurements in Fig. 2(b), is achieved by adjusting 4 parameters simultaneously: the light-matter coupling $g = 17.5 \pm 0.5$ μeV, the emission rate in other modes than the cavity mode $\gamma_{\mathrm{sp}} = 0.9 \pm 0.2$ μeV, the standard deviation of the QD frequency $\sigma_{\mathrm{SW}} = 2.6 \pm 0.5$ μeV, and an additional QD pure dephasing rate $\gamma^* = 0.4 \pm 0.1$ μeV for the trion transitions [37]. Overall, while the time dependence of correlators provides information on the dynamics of the spin itself, i.e., spin noise, their absolute amplitude provides information on the environmental noise [34,37] inducing a broadening of the optical transitions. Measuring absolute correlator amplitudes is also a good way to access the measurement back-action induced by a single detected photon [51]. Perfect back-action, which is crucial for spin-photon entanglement protocols [56], would correspond to $C_\theta(0) = 1$, which could be reached through a strong reduction of spectral fluctuations [33].

In conclusion, we show that single-spin SNS can be performed with single-photon detectors, through cross-correlations between detection events, taking advantage of giant polarization rotations in pillar-based structures. The fundamental difference, compared to frequency-domain measurements with balanced photodiodes [28–30], is the use of quantum optics tools [51]. This relates our approach to the framework of random-time quantum measurements [57], allowing higher-order correlation measurements using time-tagging data [58]. A number of phenomena could be studied thanks to the versatility of the approach, which could be extended to various combinations of detectors and measurement bases. This includes cross-correlations in the HV basis [37], which allow maximizing the sensitivity to the charge dynamics while minimizing the sensitivity to the spin dynamics. Our approach could also be extended to bandwidths above 10 GHz, limited only by the temporal jitter of photon detection, allowing the direct monitoring of Larmor precessions, electron spin relaxation and decoherence, or damped Rabi oscillations between the ground and trion states [51]. It is also the starting point for fundamental studies quantitatively addressing the quantum back-action induced by photon detection [51,57,59]. Ultimately, giant optical rotations could be exploited with sub-nanosecond pulses, to achieve single-shot spin readout [60,61] using few photons, or to demonstrate the deterministic entanglement of a spin qubit with single incoming or reflected photons [56,62].

Acknowledgments—We are thankful to D. S. Smirnov for inspiring discussions. This work was partially supported by the Paris Ile-de-France Région in the framework of DIM SIRTEQ, the European Union's Horizon 2020 Research and Innovation Programme QUDOT-TECH under the Marie Sklodowska-Curie Grant Agreement No. 861097, the European Union's Horizon 2020 FET OPEN project QLUSTER (Grant ID 862035), the French National Research Agency (ANR) project SPIQE (ANR- 14-CE32-0012), and a public grant overseen by the French National Research Agency (ANR) as part of the "Investissements d'Avenir" programme (Labex NanoSaclay, reference: ANR-10-LABX-0035). This work was done within the C2N micro nanotechnologies platforms and partly supported by the RENATECH network and the General Council of Essonne.

[1] T. D. Ladd, F. Jelezko, R. Laflamme, Y. Nakamura, C. Monroe, and J. L. O'Brien, Quantum computers, Nature (London) **464**, 45 (2010).

[2] N. Gisin and R. Thew, Quantum communication, Nat. Photonics **1**, 165 (2007).
[3] C. L. Degen, F. Reinhard, and P. Cappellaro, Quantum sensing, Rev. Mod. Phys. **89**, 035002 (2017).
[4] E. B. Aleksandrov and V. S. Zapasskii, Zh. Eksp. Teor. Fiz. **81**, 132 (1981).
[5] S. Crooker, D. Rickel, A. Balatsky, and D. Smith, Spectroscopy of spontaneous spin noise as a probe of spin dynamics and magnetic resonance, Nature (London) **431**, 49 (2004).
[6] M. Oestreich, M. Römer, R. J. Haug, and D. Hägele, Spin noise spectroscopy in GaAs, Phys. Rev. Lett. **95**, 216603 (2005).
[7] V. S. Zapasskii, Spin-noise spectroscopy: From proof of principle to applications, Adv. Opt. Photonics **5**, 131 (2013).
[8] N. A. Sinitsyn and Y. V. Pershin, The theory of spin noise spectroscopy: A review, Rep. Prog. Phys. **79**, 106501 (2016).
[9] G. M. Müller, M. Römer, J. Hübner, and M. Oestreich, Gigahertz spin noise spectroscopy in n-doped bulk GaAs, Phys. Rev. B **81**, 121202(R) (2010).
[10] F. Berski, H. Kuhn, J. G. Lonnemann, J. Hübner, and M. Oestreich, Ultrahigh bandwidth spin noise spectroscopy: Detection of large g-factor fluctuations in highly-n-doped GaAs, Phys. Rev. Lett. **111**, 186602 (2013).
[11] S. Cronenberger and D. Scalbert, Quantum limited heterodyne detection of spin noise, Rev. Sci. Instrum. **87**, 093111 (2016).
[12] M. Y. Petrov, A. N. Kamenskii, V. S. Zapasskii, M. Bayer, and A. Greilich, Increased sensitivity of spin noise spectroscopy using homodyne detection in n-doped GaAs, Phys. Rev. B **97**, 125202 (2018).
[13] S. Cronenberger, C. Abbas, D. Scalbert, and H. Boukari, Spatiotemporal spin noise spectroscopy, Phys. Rev. Lett. **123**, 017401 (2019).
[14] L. Yang, P. Glasenapp, A. Greilich, D. Reuter, A. D. Wieck, D. R. Yakovlev, M. Bayer, and S. A. Crooker, Two-colour spin noise spectroscopy and fluctuation correlations reveal homogeneous linewidths within quantum-dot ensembles, Nat. Commun. **5**, 4949 (2014).
[15] F. Li, S. A. Crooker, and N. A. Sinitsyn, Higher-order spin-noise spectroscopy of atomic spins in fluctuating external fields, Phys. Rev. A **93**, 033814 (2016).
[16] F. Li, Y. V. Pershin, V. A. Slipko, and N. A. Sinitsyn, Nonequilibrium spin noise spectroscopy, Phys. Rev. Lett. **111**, 067201 (2013).
[17] P. Glasenapp, N. A. Sinitsyn, L. Yang, D. G. Rickel, D. Roy, A. Greilich, M. Bayer, and S. A. Crooker, Spin noise spectroscopy beyond thermal equilibrium and linear response, Phys. Rev. Lett. **113**, 156601 (2014).
[18] V. V. Belykh, D. R. Yakovlev, and M. Bayer, Optical detection of electron spin dynamics driven by fast variations of a magnetic field: A simple method to measure T_1, T_2, and T_2^* in semiconductors, Sci. Rep. **10**, 13155 (2020).
[19] V. Guarrera, R. Gartman, G. Bevilacqua, and W. Chalupczak, Spin-noise spectroscopy of a noise-squeezed atomic state, Phys. Rev. Res. **3**, L032015 (2021).
[20] M. Atatüre, J. Dreiser, A. Badolato, and A. Imamoglu, Observation of Faraday rotation from a single confined spin, Nat. Phys. **3**, 101 (2007).
[21] A. Bechtold, D. Rauch, F. Li, T. Simmet, P.-L. Ardelt, A. Regler, K. Müller, N. A. Sinitsyn, and J. J. Finley, Three-stage decoherence dynamics of an electron spin qubit in an optically active quantum dot, Nat. Phys. **11**, 1005 (2015).
[22] D. Cogan, O. Kenneth, N. H. Lindner, G. Peniakov, C. Hopfmann, D. Dalacu, P. J. Poole, P. Hawrylak, and D. Gershoni, Depolarization of electronic spin qubits confined in semiconductor quantum dots, Phys. Rev. X **8**, 041050 (2018).
[23] G. N. Nguyen, C. Spinnler, M. R. Hogg, L. Zhai, A. Javadi, C. A. Schrader, M. Erbe, M. Wyss, J. Ritzmann, H.-G. Babin, A. D. Wieck, A. Ludwig, and R. J. Warburton, Enhanced electron-spin coherence in a GaAs quantum emitter, Phys. Rev. Lett. **131**, 210805 (2023).
[24] L. Zaporski, N. Shofer, J. H. Bodey, S. Manna, G. Gillard, M. H. Appel, C. Schimpf, S. F. C. da Silva, J. Jarman, G. Delamare, G. Park, U. Haeusler, E. A. Chekhovich, A. Rastelli, D. A. Gangloff, M. Atatüre, and C. L. Gall, Ideal refocusing of an optically active spin qubit under strong hyperfine interactions, Nat. Nanotechnol. **18**, 257 (2023).
[25] R. Giri, S. Cronenberger, M. Vladimirova, D. Scalbert, K. V. Kavokin, M. M. Glazov, M. Nawrocki, A. Lemaître, and J. Bloch, Giant photoinduced Faraday rotation due to the spin-polarized electron gas in a *n*-GaAs microcavity, Phys. Rev. B **85**, 195313 (2012).
[26] S. V. Poltavtsev, I. I. Ryzhov, M. M. Glazov, G. G. Kozlov, V. S. Zapasskii, A. V. Kavokin, P. G. Lagoudakis, D. S. Smirnov, and E. L. Ivchenko, Spin noise spectroscopy of a single quantum well microcavity, Phys. Rev. B **89**, 081304 (R) (2014).
[27] R. V. Cherbunin, M. Vladimirova, K. V. Kavokin, A. V. Mikhailov, N. E. Kopteva, P. G. Lagoudakis, and A. V. Kavokin, Significant photoinduced Kerr rotation achieved in semiconductor microcavities, Phys. Rev. B **91**, 205308 (2015).
[28] R. Dahbashi, J. Hübner, F. Berski, K. Pierz, and M. Oestreich, Optical spin noise of a single hole spin localized in an (InGa)As quantum dot, Phys. Rev. Lett. **112**, 156601 (2014).
[29] J. Wiegand, D. S. Smirnov, J. Hübner, M. M. Glazov, and M. Oestreich, Spin and reoccupation noise in a single quantum dot beyond the fluctuation-dissipation theorem, Phys. Rev. B **97**, 081403(R) (2018).
[30] T.-J. Sun, P. Sterin, L. Lengert, C. Nawrath, M. Jetter, P. Michler, Y. Ji, J. Hübner, and M. Oestreich, Non-equilibrium spin noise spectroscopy of a single quantum dot operating at fiber telecommunication wavelengths, J. Appl. Phys. **131**, 065703 (2022).
[31] C. Arnold, J. Demory, V. Loo, A. Lemaître, I. Sagnes, M. Glazov, O. Krebs, P. Voisin, P. Senellart, and L. Lanco, Macroscopic rotation of photon polarization induced by a single spin, Nat. Commun. **6**, 6236 (2015).
[32] P. Androvitsaneas, A. B. Young, J. M. Lennon, C. Schneider, S. Maier, J. J. Hinchliff, G. S. Atkinson, E. Harbord, M. Kamp, S. Höfling, J. G. Rarity, and R. Oulton, Efficient quantum photonic phase shift in a low q-factor regime, ACS Photonics **6**, 429 (2019).
[33] E. Mehdi, M. Gundín-Martinez, C. Millet, N. Somaschi, A. Lemaître, I. Sagnes, L. L. Gratiet, D. Fioretto, N. Belabas, O. Krebs, P. Senellart, and L. Lanco, Giant optical polar-

isation rotations induced by a single quantum dot spin, Nat. Commun. **15**, 598 (2024).
[34] A. V. Kuhlmann, J. Houel, A. Ludwig, L. Greuter, D. Reuter, A. D. Wieck, M. Poggio, and R. J. Warburton, Charge noise and spin noise in a semiconductor quantum device, Nat. Phys. **9**, 570 (2013).
[35] P. Hilaire, C. Millet, J. C. Loredo, C. Antón, A. Harouri, A. Lemaître, I. Sagnes, N. Somaschi, O. Krebs, P. Senellart, and L. Lanco, Deterministic assembly of a charged-quantum-dot–micropillar cavity device, Phys. Rev. B **102**, 195402 (2020).
[36] P.-L. Ardelt, T. Simmet, K. Müller, C. Dory, K. A. Fischer, A. Bechtold, A. Kleinkauf, H. Riedl, and J. J. Finley, Controlled tunneling-induced dephasing of Rabi rotations for high-fidelity hole spin initialization, Phys. Rev. B **92**, 115306 (2015).
[37] See Supplemental Material at http://link.aps.org/supplemental/10.1103/PhysRevLett.134.036902, which includes Refs. [38–46], for additional information about the experimental methods and a detailed discussion of the numerical simulations.
[38] A. Dousse, L. Lanco, J. Suffczyński, E. Semenova, A. Miard, A. Lemaître, I. Sagnes, C. Roblin, J. Bloch, and P. Senellart, Controlled light-matter coupling for a single quantum dot embedded in a pillar microcavity using far-field optical lithography, Phys. Rev. Lett. **101**, 267404 (2008).
[39] N. Somaschi, V. Giesz, L. De Santis, J. C. Loredo, M. P. Almeida, G. Hornecker, S. L. Portalupi, T. Grange, C. Antón, J. Demory, C. Gómez, I. Sagnes, N. D. Lanzillotti-Kimura, A. Lemaître, A. Auffeves, A. G. White, L. Lanco, and P. Senellart, Near-optimal single-photon sources in the solid state, Nat. Photonics **10**, 340 (2016).
[40] S. M. Tan, A computational toolbox for quantum and atomic optics, J. Opt. B **1**, 424 (1999).
[41] *Quantum Optics*, edited by D. Walls and G. J. Milburn (Springer, Berlin, Heidelberg, 2008).
[42] H. S. Nguyen, G. Sallen, C. Voisin, P. Roussignol, C. Diederichs, and G. Cassabois, Ultra-coherent single photon source, Appl. Phys. Lett. **99**, 261904 (2011).
[43] C. Matthiesen, A. N. Vamivakas, and M. Atatüre, Subnatural linewidth single photons from a quantum dot, Phys. Rev. Lett. **108**, 093602 (2012).
[44] N. Coste, M. Gundin, D. A. Fioretto, S. E. Thomas, C. Millet, E. Mehdi, N. Somaschi, M. Morassi, M. Pont, A. Lemaître, N. Belabas, O. Krebs, L. Lanco, and P. Senellart, Probing the dynamics and coherence of a semiconductor hole spin via acoustic phonon-assisted excitation, Quantum Sci. Technol. **8**, 025021 (2023).
[45] J. H. Prechtel, A. V. Kuhlmann, J. Houel, A. Ludwig, S. R. Valentin, A. D. Wieck, and R. J. Warburton, Decoupling a hole spin qubit from the nuclear spins, Nat. Mater. **15**, 981 (2016).
[46] A. Schwan, B.-M. Meiners, A. Greilich, D. R. Yakovlev, M. Bayer, A. D. B. Maia, A. A. Quivy, and A. B. Henriques, Anisotropy of electron and hole *g*-factors in (In,Ga)As quantum dots, Appl. Phys. Lett. **99**, 221914 (2011).
[47] B. Urbaszek, X. Marie, T. Amand, O. Krebs, P. Voisin, P. Maletinsky, A. Högele, and A. Imamoglu, Nuclear spin physics in quantum dots: An optical investigation, Rev. Mod. Phys. **85**, 79 (2013).
[48] P. Hilaire, C. Antón, C. Kessler, A. Lemaître, I. Sagnes, N. Somaschi, P. Senellart, and L. Lanco, Accurate measurement of a 96% input coupling into a cavity using polarization tomography, Appl. Phys. Lett. **112**, 201101 (2018).
[49] V. Loo, C. Arnold, O. Gazzano, A. Lemaitre, I. Sagnes, O. Krebs, P. Voisin, P. Senellart, and L. Lanco, Optical nonlinearity for few-photon pulses on a quantum dot-pillar cavity device, Phys. Rev. Lett. **109**, 166806 (2012).
[50] C. Antón, P. Hilaire, C. A. Kessler, J. Demory, C. Gómez, A. Lemaître, I. Sagnes, N. D. Lanzillotti-Kimura, O. Krebs, N. Somaschi, P. Senellart, and L. Lanco, Tomography of the optical polarization rotation induced by a single quantum dot in a cavity, Optica **4**, 1326 (2017).
[51] D. S. Smirnov, B. Reznychenko, A. Auffèves, and L. Lanco, Measurement back action and spin noise spectroscopy in a charged cavity QED device in the strong coupling regime, Phys. Rev. B **96**, 165308 (2017).
[52] I. A. Merkulov, Al. L. Efros, and M. Rosen, Electron spin relaxation by nuclei in semiconductor quantum dots, Phys. Rev. B **65**, 205309 (2002).
[53] E. A. Zhukov, E. Kirstein, D. S. Smirnov, D. R. Yakovlev, M. M. Glazov, D. Reuter, A. D. Wieck, M. Bayer, and A. Greilich, Spin inertia of resident and photoexcited carriers in singly charged quantum dots, Phys. Rev. B **98**, 121304(R) (2018).
[54] P. Schering, G. S. Uhrig, and D. S. Smirnov, Spin inertia and polarization recovery in quantum dots: Role of pumping strength and resonant spin amplification, Phys. Rev. Res. **1**, 033189 (2019).
[55] D. S. Smirnov, E. A. Zhukov, D. R. Yakovlev, E. Kirstein, M. Bayer, and A. Greilich, Spin polarization recovery and Hanle effect for charge carriers interacting with nuclear spins in semiconductors, Phys. Rev. B **102**, 235413 (2020).
[56] C. Y. Hu, W. J. Munro, and J. G. Rarity, Deterministic photon entangler using a charged quantum dot inside a microcavity, Phys. Rev. B **78**, 125318 (2008).
[57] M. Sifft and D. Hägele, Random-time quantum measurements, Phys. Rev. A **107**, 052203 (2023).
[58] M. Sifft, A. Kurzmann, J. Kerski, R. Schott, A. Ludwig, A. D. Wieck, A. Lorke, M. Geller, and D. Hägele, Quantum polyspectra approach to the dynamics of blinking quantum emitters at low photon rates without binning: Making every photon count, Phys. Rev. A **109**, 062210 (2024).
[59] N. V. Leppenen, L. Lanco, and D. S. Smirnov, Quantum Zeno effect and quantum nondemolition spin measurement in a quantum dot-micropillar cavity in the strong coupling regime, Phys. Rev. B **103**, 045413 (2021).
[60] A. Delteil, W.-b. Gao, P. Fallahi, J. Miguel-Sanchez, and A. Imamoğlu, Observation of quantum jumps of a single quantum dot spin using submicrosecond single-shot optical readout, Phys. Rev. Lett. **112**, 116802 (2014).
[61] N. O. Antoniadis, M. R. Hogg, W. F. Stehl, A. Javadi, N. Tomm, R. Schott, S. R. Valentin, A. D. Wieck, A. Ludwig, and R. J. Warburton, Cavity-enhanced single-shot readout of a quantum dot spin within 3 nanoseconds, Nat. Commun. **14**, 3977 (2023).
[62] M. Maffei, B. O. Goes, S. C. Wein, A. N. Jordan, L. Lanco, and A. Auffèves, Energy-efficient quantum non-demolition measurement with a spin-photon interface, Quantum **7**, 1099 (2023).